DØ Note 5312-CONF

Search for squarks and gluinos in events with jets and missing transverse energy with the DØ detector using 1 fb^{-1} of RunIIa data

The DØ Collaboration
URL: http://www-d0.fnal.gov

(Dated: August 31, 2007)

A search for squarks and gluinos was performed on approximately 1 fb^{-1} of data from $\mathrm{p\bar{p}}$ collisions at a center-of-mass energy of 1.96 TeV, collected by the DØ detector at the Fermilab Tevatron. The topologies analyzed consist of acoplanar-jet and multijet events with large missing transverse energy. No evidence for the production of squarks or gluinos was found. Lower limits of 375 and 289 GeV were derived at the 95% C.L. on the squark and gluino masses, respectively, within the framework of minimal supergravity with $\tan\beta = 3$, $A_0 = 0$, and $\mu < 0$. Previous limits obtained by the DØ collaboration are improved by ~ 50 GeV.

Preliminary Results for Summer and Winter 2007 Conferences

I. INTRODUCTION

In models based on theories of supersymmetry, scalar quarks, or squarks, arise as partners of the quarks, and fermionic gluinos as partners of the gluons. Supersymmetric particles carry a value of -1 for R-parity, a multiplicative quantum number. In R-parity conserving theories, supersymmetric particles are therefore produced in pairs. Their decay then leads to standard model (SM) particles and, possibly via cascades, to the lightest supersymmetric particle (LSP) which is stable. The neutralinos are the supersymmetric partners of the neutral gauge and Higgs bosons, and the widely preferred LSP candidate is the lightest neutralino $\widetilde{\chi}_1^0$, which is weakly interacting and escapes detection.

At hadron colliders, the most copiously produced supersymmetric particles should be, if sufficiently light, colored particles, namely squarks and gluinos. If squarks are lighter than gluinos, they will tend to decay according to $\widetilde{\mathrm{q}} \to \mathrm{q}\widetilde{\chi}_1^0$, and their pair production will yield an acoplanar dijet topology with missing E_T carried away by the two neutralino LSP's. If gluinos are lighter than squarks, their pair production and decay via $\widetilde{\mathrm{g}} \to \mathrm{q\bar{q}}\widetilde{\chi}_1^0$ will lead to topologies containing a large number of jets and missing E_T. In generic models, squarks of the five lightest flavors tend to be of similar masses. The same is true for the supersymmetric partners of both quark helicity states. Hence, the cross section of squark pair production corresponds effectively to the sum of the productions of ten squark species.

In this note, a search for pair production of squarks and gluinos in the jets with large missing E_T ($\not\!\!E_T$) topology is reported, using approximately $1\,\mathrm{fb}^{-1}$ of data collected at a center-of-mass energy of 1.96 TeV with the upgraded DØ detector during Run IIa of the Fermilab Tevatron. Squark and gluino production is investigated in the framework of minimal supergravity (mSUGRA) [1]. The previous mass limits obtained by the DØ collaboration with 310 pb^{-1} of RunII data are 239 and 320 GeV for gluinos and squarks respectively [2]. Preliminary results were also obtained by the CDF collaboration [3]. Here and in the following, all limits are at the 95% confidence level (CL).

II. DATA AND MONTE CARLO SAMPLES

For the studies reported in this note, data collected by the DØ experiment in RunII, from April 2003 through February 2006, has been analysed. This data sample corresponds to an integrated luminosity of $0.96 \pm 0.06\,\mathrm{fb}^{-1}$ [4] after requiring data of good quality. Events were recorded using acoplanar dijet and mutijet triggers requiring missing transverse energy calculated using the sum of the jet momenta ($\not\!\!H_T = |\sum_{\mathrm{jets}} \overrightarrow{p_T}|$). The DØ trigger system consists of three levels, L1, L2, and L3 (see [5] where the DØ detector is described in detail). Events were required to have at least three calorimeter towers of size $\Delta\phi \times \Delta\eta = 0.2 \times 0.2$ with transverse energy E_T greater than 5 GeV, where ϕ is the azimuthal angle in radians and η the pseudorapidity. For the acoplanar dijet trigger, $\not\!\!H_T$ was required to be greater than 20 GeV and the acoplanarity, defined as the azimuthal angle between the two leading jets, to be less than 168.75° at L2. At L3, this trigger required $\not\!\!H_T$ to be greater than 30 GeV and the acoplanarity to be less than 170°. For the multijet trigger, at least three jets were required at L2. Events were also required to have $H_T = \sum_{\mathrm{jets}} E_T$ greater than 125 GeV and $\not\!\!H_T$ greater than 25 GeV at L3. In the last third of the data sample recorded at the highest instantaneous luminosity, additional cuts were implemented in those triggers to reduce their online rate. The minimum azimuthal angle $\Delta\phi_{\mathrm{min}}(\not\!\!H_T, \mathrm{any\,jet})$ between the $\not\!\!H_T$ direction and any jet was required to be greater than 25° at L3 for the acoplanar dijet trigger. This cut rejects events where the $\not\!\!H_T$ is aligned with a jet due to jet energy mismeasurement. For the multijet trigger, three jets with E_T greater than 20 GeV were required at L3.

Signal efficiencies and yields for standard model backgrounds involving W and Z bosons (including top production and decay) were evaluated using Monte Carlo (MC) events subjected to a full GEANT-based [6] simulation of the detector geometry and response. The $\mathrm{Z} \to \nu\bar{\nu} + \mathrm{jet(s)}$, $\mathrm{W} \to \ell\nu + \mathrm{jet(s)}$, $\mathrm{t\bar{t}}$, di-vector boson and single-top processes are expected to be the largest contributors to SM backgrounds in the jets + missing E_T topology. All $\mathrm{W/Z} + \mathrm{jet(s)}$ and $\mathrm{t\bar{t}}$ processes were generated with ALPGEN version 2.05 [7] interfaced with PYTHIA 6.319 [8] for the simulation of initial and final state radiation, and of parton hadronization. The absolute normalization of those MC was done using the inclusive W/Z and $\mathrm{t\bar{t}}$ NNLO cross-sections [9, 10]. The di-vector boson MC samples were produced with PYTHIA 6.319 [8], while the single-top MC samples were produced with COMPHEP [11].

Squark and gluino production and decay were simulated with PYTHIA 6.319. The masses and couplings of the supersymmetric particles were calculated with SUSPECT 2.3 [12] and SDECAY 1.1A [13] from the set of five mSUGRA parameters: m_0 and $m_{1/2}$, which are universal scalar and gaugino masses, and A_0, a universal trilinear coupling, all defined at the scale of grand unification; $\tan\beta$, the ratio of the vacuum expectation values of the two Higgs fields; and the sign of the Higgs-mixing mass parameter μ. To retain consistency with the previous DØ analysis [2], the following parameters were fixed: $A_0 = 0$, $\tan\beta = 3$, and $\mu < 0$. For the same reason, the production of scalar top quarks, or stops, was ignored. In the following, "squark mass" stands for the average mass of all squarks other than stops. All squark and gluino decay modes were taken into account in the simulation, including cascade decays such as $\widetilde{\mathrm{g}} \to q\bar{q}\widetilde{\chi}_2^0$ with $\widetilde{\chi}_2^0 \to \ell^+\ell^-\widetilde{\chi}_1^0$. The NLO cross sections of the various signal processes were calculated with PROSPINO 2 [14].

In all signal and SM background MC samples, the CTEQ6L1 [15] parton density functions (PDF) were used, and zero bias events from random beam crossings were overlaid on the simulated events.

III. EVENT SELECTIONS

Three benchmark scenarios were considered. At low m_0, the gluino is heavier than the squarks, and the process with the dominant cross section is $\tilde{q}\bar{\tilde{q}}$ production. A "dijet" analysis was optimized to search for events containing a pair of acoplanar jets. At high m_0, the squarks are much heavier than the gluino, and the process with the highest cross section is therefore $\tilde{g}\tilde{g}$ production. A "gluino" analysis was optimized to search for multijet events (≥ 4 jets). In the intermediate m_0 region, all squark-gluino production processes contribute to the total cross section, in particular the $\tilde{q}\tilde{g}$ process becomes relevant. A "3-jets" analysis was optimized to search for events with at least three jets. The benchmark for this analysis is the case where $m_{\tilde{q}} = m_{\tilde{g}}$.

Jets were reconstructed from the energy deposited in calorimeter towers using the Run II cone algorithm [16] with a radius of 0.5. The jet energy scale (JES) is derived from the transverse momentum balance in photon-plus-jet events. The $\not\!\!E_T$ is calculated from all calorimeter cells, and corrected for the jet energy scale.

A common event preselection was used for the three analyses to select events with substantial $\not\!\!E_T$ ($\geq$ 40 GeV) and where the two leading jets, *i.e.* those with the largest transverse energies, have $E_T \geq 35$ GeV. The acoplanarity was required to be below 165°. The longitudinal position of the primary vertex with respect to the detector center was restricted, $|z| < 60$ cm, to ensure an efficient primary vertex reconstruction [17]. The two leading jets were required to be in the central region of the calorimeter, $|\eta_{\rm det}| < 0.8$, where $\eta_{\rm det}$ is the jet pseudorapidity calculated under the assumption that the jet originates from the detector center.

The tracking capabilities of the Run II DØ detector were used to significantly reduce the QCD background with jet transverse energy mismeasurements due to a wrong vertex choice. Using good quality tracks associated to a jet within a cone of radius 0.5 around the jet-axis, the variable CPF is defined per jet as the ratio between the scalar sum of the p_T of the tracks from the jet leading to the primary vertex, divided by the scalar sum of the p_T of all the tracks from that jet. The two leading jets were required to have CPF larger than 0.85.

Different selection criteria were next applied in the three analyses, as summarized in Table I. Events passing the acoplanar dijet trigger were used in the "dijet" analysis, and events passing the multijet trigger were used in the "3-jets" and "gluino" analyses. In the "3-jets" and "gluino" analyses, a third and fourth jet were required, respectively, both with $|\eta_{\rm det}| <$2.5. The third jet must have $E_T \geq 35$ GeV and the fourth jet $E_T \geq 20$ GeV. In preparation for the final optimization, $\not\!\!E_T$ was required to be greater than 75 GeV to remove QCD background with $\not\!\!E_T$ far away from the final $\not\!\!E_T$ cut. This requirement does not bias the final selection because it is significantly lower than the final requirement. In all three analyses, a veto on isolated electrons or muons with $p_T \geq$10 GeV rejects a

TABLE I: Selection criteria for the three analyses (all energies in GeV); see the text for further details.

Preselection Cut		All Analyses	
1st jet E_T [a]		≥ 35	
2nd jet E_T [a]		≥ 35	
$\not\!\!E_T$		≥ 40	
Acoplanarity		$< 165^\circ$	
|Vertex z pos.|		< 60 cm	
Selection Cut	"dijet"	"3-jets"	"gluino"
Trigger	acoplanar dijet	multijet	multijet
3rd jet E_T [b]	–	≥ 35	≥ 35
4th jet E_T [b]	–	–	≥ 20
$\not\!\!E_T$	≥ 75	≥ 75	≥ 75
Electron veto	yes	yes	yes
Muon veto	yes	yes	yes
$\Delta\phi(\not\!\!E_T, \text{jet}_1)$	$\geq 90^\circ$	$\geq 90^\circ$	$\geq 90^\circ$
$\Delta\phi(\not\!\!E_T, \text{jet}_2)$	$\geq 50^\circ$	$\geq 50^\circ$	$\geq 50^\circ$
$\Delta\phi_{\rm min}(\not\!\!E_T, \text{any jet})$	$\geq 40^\circ$	–	–
H_T	≥ 300	≥ 400	≥ 300
$\not\!\!E_T$	≥ 225	≥ 150	≥ 100

[a] The first and second leading jets were also required to be central ($|\eta_{\rm det}| < 0.8$), and to have $CPF \geq 0.85$.
[b] The $|\eta_{\rm det}|$ cut on the third and fourth jet was < 2.5 and no CPF requirement was imposed on those jets.

large fraction of events originating from the W/Z+jets processes. The azimuthal angles between the $\not\!\!E_T$ direction and the first jet, $\Delta\phi(\not\!\!E_T, \mathrm{jet}_1)$, and the second jet, $\Delta\phi(\not\!\!E_T, \mathrm{jet}_2)$, were used to remove events where the energy of one jet was mismeasured, generating $\not\!\!E_T$ aligned with that jet. Those $\not\!\!E_T$ isolation cuts are $\Delta\phi(\not\!\!E_T, \mathrm{jet}_1) \geq 90°$ and $\Delta\phi(\not\!\!E_T, \mathrm{jet}_2) \geq 50°$. In the "dijet" analysis, QCD events were further suppressed by requiring that the minimum azimuthal angle $\Delta\phi_{\min}(\not\!\!E_T, \mathrm{any\,jet})$ between the $\not\!\!E_T$ direction and any jet with $E_T \geq 15\,\mathrm{GeV}$ be greater than 40°. Because of the higher jet multiplicity, this criterion was not used in the "3-jets" and "gluino" analyses.

The two final cuts on H_T and on $\not\!\!E_T$ were optimized by minimizing the expected upper limit on the cross section in the absence of signal. To this end, as well as for the derivation of the final results, the modified frequentist CL_s method [18] was used. The optimal cuts thus determined are given in Table I for the three analyses.

Figure 1 shows: the $\not\!\!E_T$ distribution before the two final cuts on H_T and $\not\!\!E_T$ and without the intermediate cut on $\not\!\!E_T$ at 75 GeV in the "dijet" analysis; the $\Delta\phi_{\min}(\not\!\!E_T, \mathrm{any\,jet})$ distribution in the "dijet" analysis before applying the $\not\!\!E_T$ isolation cuts; the H_T distribution after applying all the "3-jets" analysis criteria except the one on H_T; and the $\not\!\!E_T$ distribution after applying all the "gluino" analysis criteria except the intermediate cut on $\not\!\!E_T$ at 75 GeV and the final cut on $\not\!\!E_T$.

IV. RESULTS

The numbers of events selected by each analysis are reported in Table II, as well as the numbers of background events expected. The QCD background contribution, estimated from an exponential fit to the $\not\!\!E_T$ distribution below 60 GeV, after subtraction of the SM background processes, and extrapolated above the chosen $\not\!\!E_T$ cut value, was estimated to be negligible at the end of the three analyses. Five events were selected by the "dijet" analysis, six by the "3-jets" analysis, and 34 by the "gluino" analysis. The total expected background contributions are 7.5, 6.1 and 33.4 events, respectively. The main background contributions are due to $\mathrm{Z} \to \nu\bar{\nu}$ + jets, $\mathrm{W} \to l\nu$ + jets, and $\mathrm{t\bar{t}} \to \mathrm{b\bar{b}}\, q\bar{q}' l\nu$.

The three analyses were run over signal MC samples generated in the gluino-squark mass plane to compute signal efficiencies. They are reported in Table III for the three benchmark signals used to optimize the three analyses.

Systematic uncertainties on the SM background expectations and signal efficiencies were evaluated. The uncertainty coming from the JES corrections is one of the most important. It is typically of the order of 10% to 15% for the SM backgrounds and 6% to 11% for the signal efficiencies. The uncertainties on the jet energy resolution, on the jet CPF, and on the jet reconstruction and identification efficiencies lead to systematic uncertainties of 5%, 7% and 7% in the "dijet," "3-jets," and "gluino" analyses, respectively. The trigger efficiencies were found to be 96 ± 2% for the event samples surviving all analysis cuts. The uncertainty on the determination of the luminosity is 6.1% [4]. All of these uncertainties are fully correlated between signal and SM backgrounds. A 15% systematic uncertainty was set on the SM background cross sections. The uncertainty on the signal acceptance due to the PDF choice was determined to be 6% using the forty-eigenvector basis of the CTEQ6.1M PDF set [15].

To improve the sensitivity, the three analyses described previously were combined when computing the limits. To do so, 7 independent and exclusive combinations with no overlaps based on logical "ANDs" between the "dijet", "3-jets"

TABLE II: Definition of the analysis combinations, and number of events observed in the data and expected from the SM for all the event selections ("-" means not considered, "no" means vetoed).

Name	"dijet"	"3-jets"	"gluino"	Data	SM events expected
"dijet"	yes	-	-	5	7.47 ± 1.06 (stat.) $^{+1.32}_{-1.02}$ (syst.)
"3-jets"	-	yes	-	6	6.10 ± 0.37 (stat.) $^{+1.26}_{-1.16}$ (syst.)
"gluino"	-	-	yes	34	33.35 ± 0.81 (stat.) $^{+5.56}_{-4.92}$ (syst.)
combination 1	yes	no	no	5	6.10 ± 1.04 (stat.) $^{+1.17}_{-0.73}$ (syst.)
combination 2	no	yes	no	1	1.09 ± 0.14 (stat.) $^{+0.17}_{-0.22}$ (syst.)
combination 3	no	no	yes	29	27.78 ± 0.73 (stat.) $^{+4.39}_{-3.84}$ (syst.)
combination 4	yes	yes	no	0	0.22 ± 0.07 (stat.) $^{+0.02}_{-0.06}$ (syst.)
combination 5	yes	no	yes	0	0.78 ± 0.14 (stat.) $^{+0.12}_{-0.16}$ (syst.)
combination 6	no	yes	yes	5	4.42 ± 0.32 (stat.) $^{+1.01}_{-0.83}$ (syst.)
combination 7	yes	yes	yes	0	0.37 ± 0.11 (stat.) $^{+0.07}_{-0.13}$ (syst.)
global "OR"		-		40	40.76 ± 1.33 (stat.) $^{+6.91}_{-5.88}$ (syst.)

and "gluino" analyses were performed as summarized in Table II. The number of events selected in the data, and expected in the MC are also provided. The number of observed events is in good agreement with the SM expectations for all the event selections. Applying a logical "OR" between the "dijet", "3-jets" and "gluino" analyses, 40 events are selected in the data and the simulation predicts 40.8 ± 1.3 (stat.) $^{+6.9}_{-5.9}$ (syst.). Event displays of the acoplanar dijet and multijet events with the highest $\not\!\!E_T$ are shown in Figs. 2 and 3, respectively. Their kinematic properties are also given in Table IV.

The signal cross sections are very sensitive to the PDF choice and to the renormalization and factorization scale, $\mu_{\rm rf}$. The nominal NLO cross sections, $\sigma_{\rm nom}$, were computed with the CTEQ6.1M PDF and for $\mu_{\rm rf} = Q$, where Q was taken to be equal to $m_{\tilde{\rm g}}$ for $\tilde{\rm g}\tilde{\rm g}$ production, $m_{\tilde{\rm q}}$ for $\tilde{\rm q}\tilde{\rm q}$ and $\tilde{\rm q}\bar{\tilde{\rm q}}$ productions, and $(m_{\tilde{\rm q}} + m_{\tilde{\rm g}})/2$ for $\tilde{\rm q}\tilde{\rm g}$ production. The uncertainty due to the choice of PDF was determined using the full set of CTEQ6.1M eigenvectors, with the individual uncertainties added in quadrature. The effect on the nominal signal cross sections, which varies between 15% and 50%, is dominated by the large uncertainty on the gluon distribution at high x. The effect of the renormalization and factorization scale was studied by calculating the signal cross sections for $\mu_{\rm rf} = Q$, $\mu_{\rm rf} = Q/2$ and $\mu_{\rm rf} = 2 \times Q$. The factor two on this scale reduces or increases the nominal signal cross sections by 15−20%. The PDF and $\mu_{\rm rf}$ effects were added in quadrature to compute minimum, $\sigma_{\rm min}$, and maximum, $\sigma_{\rm max}$, signal cross sections.

Figure 4 shows the observed and expected upper limits at the 95% C.L. on squark-gluino production cross sections for the three benchmark scenarios. In the limit computation, the seven combinations were treated as seven independent channels, with correlations of systematic uncertainties taken into account. Mass limits were computed for the three hypotheses on the signal cross sections: nominal, minimum, and maximum (cf Fig. 4).

From the excluded domain in the gluino-squark mass plane shown in Figure 5, absolute lower limits on the squark and gluino masses, i.e. the gluino mass limit is valid for any squark mass and vice versa, are obtained. For the most conservative hypothesis, $\sigma_{\rm min}$, these limits are 375 GeV and 289 GeV on the squark and gluino mass, respectively. The corresponding expected limits are 366 GeV and 290 GeV. Table V summarizes these limits as a function of the signal cross section hypothesis. Limits were also derived for the particular case $m_{\tilde{\rm q}} = m_{\tilde{\rm g}}$. For $\sigma_{\rm min}$, squark and gluino masses below 383 GeV are excluded, while the expected limit is 379 GeV. The observed limit becomes 402 GeV for $\sigma_{\rm nom}$, and 422 GeV for $\sigma_{\rm max}$. Previous limits [2] are improved by ~ 50 GeV.

TABLE III: For each analysis, information on the signal for which it was optimized (with $\tan\beta = 3$, $A_0 = 0$, $\mu < 0$): m_0, $m_{1/2}$, $m_{\tilde{\rm g}}$, $m_{\tilde{\rm q}}$, nominal NLO cross section, and signal efficiency. The uncertainty on the signal cross section corresponds to the effect of the PDF uncertainties and of varying $\mu_{\rm rf}$ by a factor of two.

Analysis	$(m_0, m_{1/2})$ GeV	$(m_{\tilde{\rm g}}, m_{\tilde{\rm q}})$ GeV	σ pb	$\epsilon_{\rm sig.}$ %
"dijet"	(25,165)	(416,375)	$0.129^{+0.047}_{-0.034}$	7.05 ± 0.39 (stat.) $^{+0.96}_{-0.88}$ (syst.)
"3-jets"	(188,145)	(380,380)	$0.146^{+0.066}_{-0.044}$	6.66 ± 0.37 (stat.) $^{+1.11}_{-1.01}$ (syst.)
"gluino"	(500,100)	(296,542)	$0.405^{+0.185}_{-0.123}$	5.74 ± 0.35 (stat.) $^{+0.81}_{-0.72}$ (syst.)

TABLE IV: Kinematic properties of the acoplanar dijet and multijet events with the largest missing E_T. Energies and momenta are in GeV and angles in radians.

Acoplanar dijet candidate			
		η	ϕ
$\not\!\!E_T$	368		4.10
H_T	489		
E_T jet 1	282	−0.18	1.52
E_T jet 2	174	−0.37	0.12
E_T jet 3	32.5	−0.99	6.17
Multijet candidate			
		η	ϕ
$\not\!\!E_T$	321		4.73
H_T	464		
E_T jet 1	254	0.05	1.52
E_T jet 2	76.8	−0.38	0.12
E_T jet 3	67.2	1.30	4.67
E_T jet 4	66.2	0.67	1.35

The results of this analysis also constrain the mSUGRA parameters at the grand unification scale. Figure 6 shows the excluded regions in the $(m_0, m_{1/2})$ plane for $\tan\beta = 3$, $A_0 = 0$, $\mu < 0$. Limits from the LEP2 chargino and slepton searches [26] are improved for m_0 values between 75 and 250 GeV and for $m_{1/2}$ values between 125 and 165 GeV.

TABLE V: Lower limits at the 95% C.L. on the squark and gluino masses (in GeV) as a function of the choice of signal cross section hypothesis as defined in the text. The numbers in parentheses correspond to the expected limits. These limits are valid for the mSUGRA parameters: $\tan\beta = 3$, $A_0 = 0$, $\mu < 0$.

Hypothesis	Gluino mass	Squark mass
$\sigma_{\rm min}$	289 (290)	375 (366)
$\sigma_{\rm nom}$	309 (311)	391 (384)
$\sigma_{\rm max}$	329 (332)	405 (397)

Recently, the CDF experiment released an update of the squark-gluino analysis using a data sample of $1.4\,{\rm fb}^{-1}$ [3]. There are several differences between the DØ and CDF analyses. The value of $\tan\beta$ used by DØ is 3, and 5 by CDF. Furthermore, the SUSPECT 2.3 [12] and SDECAY 1.1A [13] programs are used in this analysis, while CDF is using ISASUSY [19]. However, the effects of $\tan\beta$ and program choice on the sparticle mass spectrum are small. In the DØ analysis, ISR and FSR effects on the signal acceptance were studied recently. PYTHIA parameters controlling the QCD scales Λ_{QCD} and the maximal allowed virtualities Q^2_{max} used in the simulation of the space-like and time-like parton showers were varied according to the recommendations available in [20]. The ISR/FSR systematic uncertainty on the signal efficiencies was found to be 6%. It has been checked that this uncertainty is sufficiently small compared to other uncertainties, and that it does not affect the limits reported above. For a consistent comparison between the DØ and CDF results, this systematic uncertainty from ISR/FSR is included in the following. The main difference between the DØ and CDF analyses resides in the final limit computation. CDF uses in the CL_s computation the systematic uncertainties on the signal cross sections due to the PDF choice and to the renormalization and factorization scale. This procedure is less conservative than the one adopted here when mass limits are computed for the $\sigma_{\rm min}$ hypothesis. Figure 7 shows a comparison of the CDF and DØ excluded region in the gluino-squark mass plane using in both cases the CDF prescription for the limit computation. Table VI shows the corresponding absolute lower limits on the squark and gluino masses.

TABLE VI: Comparison of the lower limits at the 95% C.L. on the squark and gluino masses (in GeV) obtained by CDF and DØ. Limits for the particular case $m_{\tilde{\rm q}} = m_{\tilde{\rm g}}$ are also quoted. Signal systematic uncertainties due to the PDF choice and to the renormalization and factorization scale are included in the limit computation in both cases. These limits are valid for the mSUGRA parameters $\tan\beta = 3$, $A_0 = 0$, $\mu < 0$ for DØ, and $\tan\beta = 5$, $A_0 = 0$, $\mu < 0$ for CDF.

	Gluino mass	Squark mass	$m_{\tilde{\rm q}} = m_{\tilde{\rm g}}$
DØ	302 (303)	385 (375)	392 (388)
CDF	276 (276)	375 (374)	380 (384)

V. CONCLUSION

Signals of squark and gluino production were searched for in $1\,{\rm fb}^{-1}$ of DØ data recorded at a center-of-mass energy of 1.96 TeV in events with jets and large missing E_T. No deviation from standard model expectations was observed. Limits at 95% confidence level were set on squark and gluino masses in the mSUGRA model. For $\tan\beta = 3$, $A_0 = 0$ and $\mu < 0$, the mass limits on the squark and gluino masses are 375 GeV and 289 GeV respectively for the choice of PDF and of the renormalization and factorization scale which corresponds to the minimum signal cross section hypothesis. For the default value of the renormalization and factorization scale and of the PDF, those limits are 391 GeV and 309 GeV. These results improve previous limits on squark and gluino masses in the mSUGRA model by ~ 50 GeV. Those are the most constraining direct limits on the squark and gluino masses to date.

Acknowledgments

We thank the staffs at Fermilab and collaborating institutions, and acknowledge support from the DOE and NSF (USA); CEA and CNRS/IN2P3 (France); FASI, Rosatom and RFBR (Russia); CAPES, CNPq, FAPERJ, FAPESP and FUNDUNESP (Brazil); DAE and DST (India); Colciencias (Colombia); CONACyT (Mexico); KRF and KOSEF (Korea); CONICET and UBACyT (Argentina); FOM (The Netherlands); PPARC (United Kingdom); MSMT (Czech Republic); CRC Program, CFI, NSERC and WestGrid Project (Canada); BMBF and DFG (Germany); SFI (Ireland); The Swedish Research Council (Sweden); Research Corporation; Alexander von Humboldt Foundation; and the Marie Curie Program.

---

[1] H.P. Nilles, Phys. Rep. **110** (1984) 1.
[2] DØ Collaboration, V.M. Abazov *et al.*, Phys. Lett. **B638**, (2006) 119.
[3] CDF Collaboration, *"Search for Gluino and Squark Production in Multijets plus missing E_T Final States"*, talk given by X. Portell at the EPS 2007 conference.
[4] T. Andeen *et. al.*, FERMILAB-TM-2365-E (2006), in preparation.
[5] DØ Collaboration, V.M. Abazov *et al.*, Nucl. Instrum. Meth. A **565**, 463 (2006).
[6] R. Brun and F. Carminati, CERN Program Library Long Writeup W5013, 1993 (unpublished).
[7] M.L. Mangano *et al.*, JHEP **0307** (2003) 001.
[8] T. Sjöstrand *et al.*, Computer Phys. Commun. **135** (2001) 238.
[9] R. Hamberg, W. L. van Neerven and T. Matsuura, Nucl. Phys. B **359**, 343 (1991) [Erratum-ibid. B **644**, 403 (2002)].
[10] N. Kidonakis and R. Vogt, Int. J. Mod. Phys. A **20**, 3171 (2005).
[11] A.Pukhov *et al.*, Preprint INP MSU 98-41/542, hep-ph/9908288.
[12] A. Djouadi, J. L. Kneur and G. Moultaka, *"SuSpect: A Fortran code for the supersymmetric and Higgs particle spectrum in the MSSM,"* hep-ph/0211331.
[13] M. Mühlleitner, A. Djouadi, and Y. Mambrini, *"SDECAY: a Fortran code for the decays of the supersymmetric particles in the MSSM,"* Comput. Phys. Commun. **168** (2005) 46.
[14] W. Beenakker, R. Hopker and M. Spira, Nucl. Phys. B **492** (1997) 51.
[15] J. Pumplin *et al.*, JHEP **0207** (2002) 012,
D. Stump *et al.*, JHEP **0310** (2003) 046.
[16] G.C. Blazey *et al.*, in *Proceedings of the Workshop: "QCD and Weak Boson Physics in Run II,"* edited by U. Baur, R.K. Ellis, and D. Zeppenfeld (Fermilab, Batavia, IL, 2000), p. 47; see Sec. 3.5 for details.
[17] DØ Collaboration, V.M. Abazov *et al.*, Phys. Rev. D **74** (2006) 112004.
[18] T. Junk, Nucl. Instrum. Methods in Phys. Res. A **434**, 435 (1999); A. Read, in *"1st Workshop on Confidence Limits,"* CERN Report No. CERN-2000-005, 2000.
[19] H. Baer, F. E. Paige, S. D. Protopopescu and X. Tata, arXiv:hep-ph/9305342.
[20] P. Bartalini, R. Chierici, and A. de Roeck, CMS-NOTE-2005-013.
[21] DØ Collaboration, B. Abbott *et al.*, Phys. Rev. Lett. **83** (1999) 4937.
[22] CDF Collaboration, T. Affolfer *et al.*, Phys. Rev. Lett. **88** (2002) 041801.
[23] UA1 Collaboration, C. Albajar *et al.*, Phys. Lett. **B198** (1987) 261.
[24] UA2 Collaboration, J. Alitti *et al.*, Phys. Lett. **B235** (1990) 363.
[25] DØ Collaboration, S. Abachi *et al.*, Phys. Rev. Lett. **75** (1995) 618.
[26] LEP SUSY Working Group for the ALEPH, DELPHI, L3 and OPAL collaborations, http://lepsusy.web.cern.ch/lepsusy/.

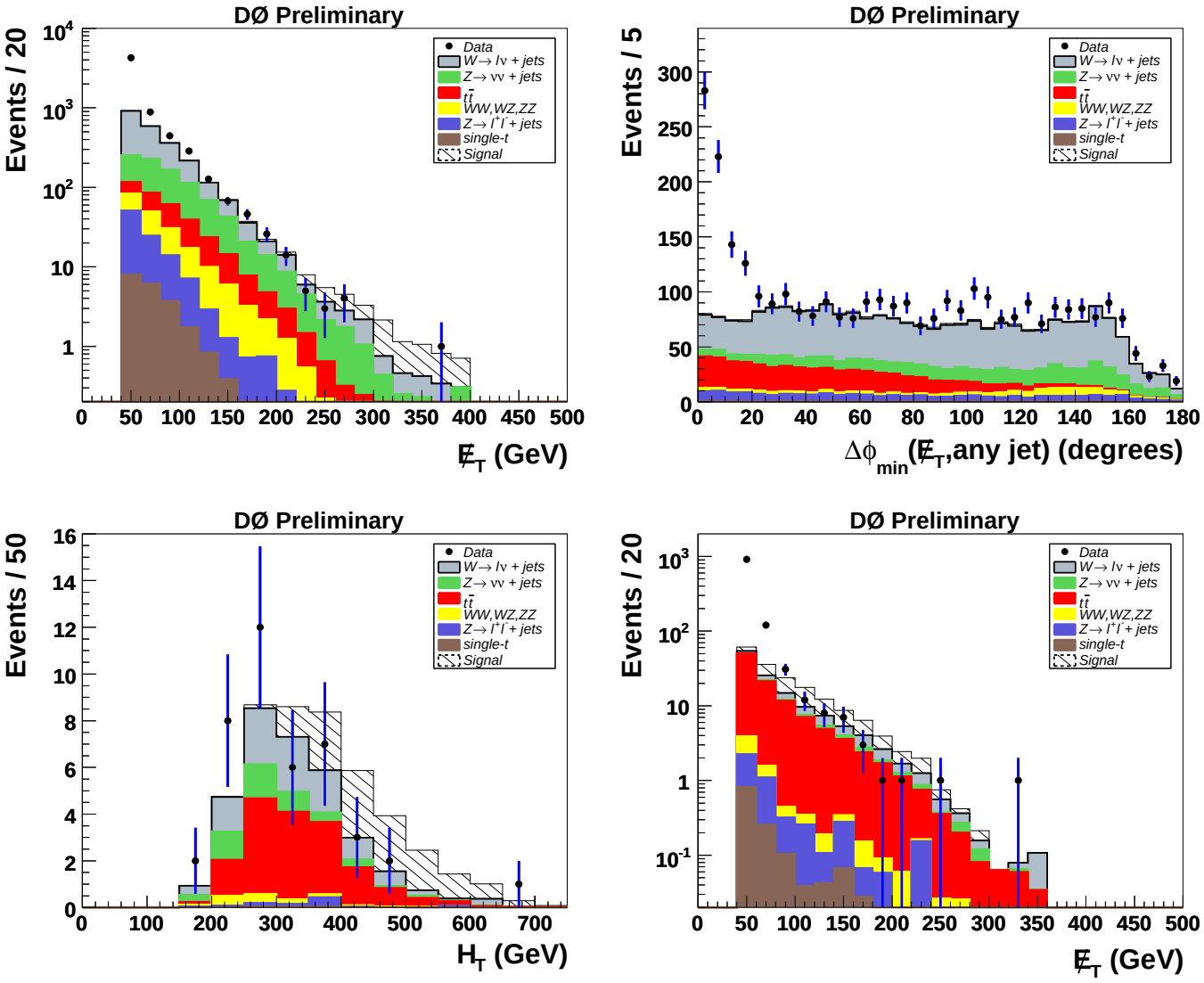

FIG. 1: Distribution of $\not\!\!E_T$ before the two final cuts on H_T and $\not\!\!E_T$ and without the intermediate cut on $\not\!\!E_T$ at 75 GeV in the "dijet" analysis (top left), distribution of $\Delta\phi_{\rm min}(\not\!\!E_T, \text{any jet})$ in the "dijet" analysis before cutting on that variable (top right), distribution of H_T after applying all the "3-jets" analysis criteria except the one on H_T (bottom left), and distribution of $\not\!\!E_T$ after applying all the "gluino" analysis criteria except the intermediate cut on $\not\!\!E_T$ at 75 GeV and final cut on $\not\!\!E_T$ (bottom right) for data (points with error bars), for non-QCD standard model background (full histograms), and for signal Monte Carlo (hashed histogram on top of SM). The MC signals used in these histograms are $(m_0, m_{1/2}) = (25, 165)$ GeV, $m_{\tilde{\rm q}} = m_{\tilde{\rm g}} = 380$ GeV, and $(m_0, m_{1/2}) = (500, 100)$ GeV for the "dijet", "3-jets" and "gluino" analyses, respectively. The excess of data at low values of $\not\!\!E_T$, H_T, and $\Delta\phi_{\rm min}(\not\!\!E_T, \text{any jet})$ is due to the QCD background which is not included in the SM background simulation.

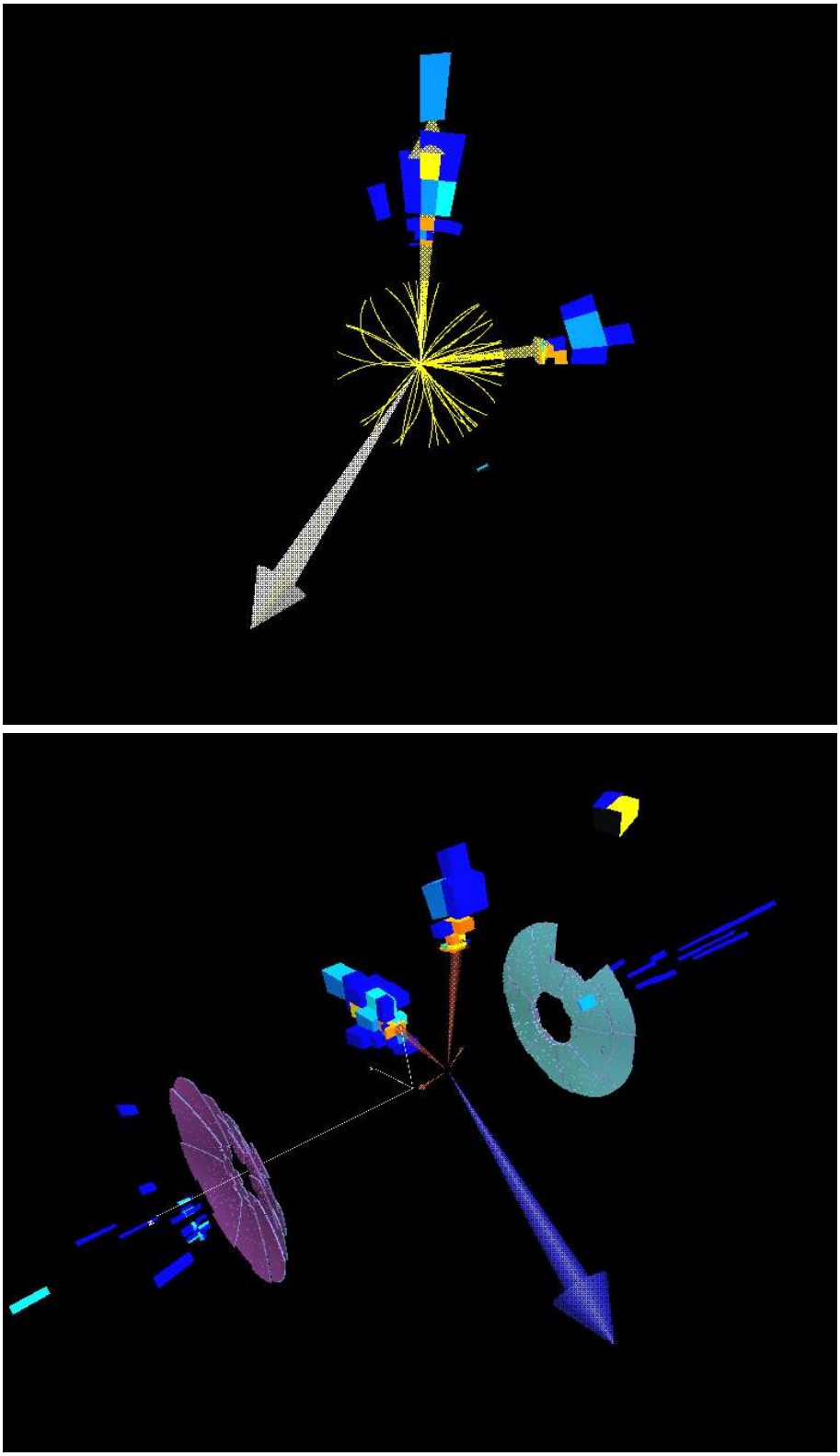

FIG. 2: Event displays of the acoplanar dijet candidate with the largest $\not\!\!E_T$. The kinematic properties of this event are given in Table IV. Arrows pointing to clusters in the calorimeter correspond to the reconstructed jets, and the isolated arrow corresponds to the $\not\!\!E_T$.

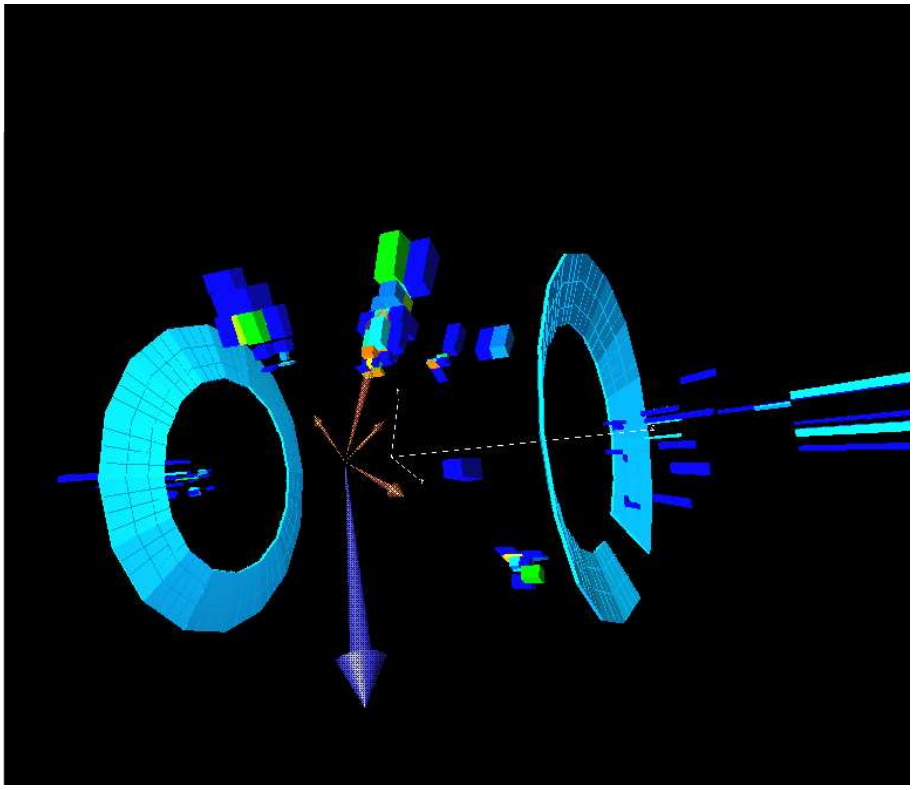

FIG. 3: Event display of the multijet candidate with the largest $\not\!\!E_T$. The kinematic properties of this event are given in Table IV. Arrows pointing to clusters in the calorimeter correspond to the reconstructed jets, and the isolated arrow corresponds to the $\not\!\!E_T$.

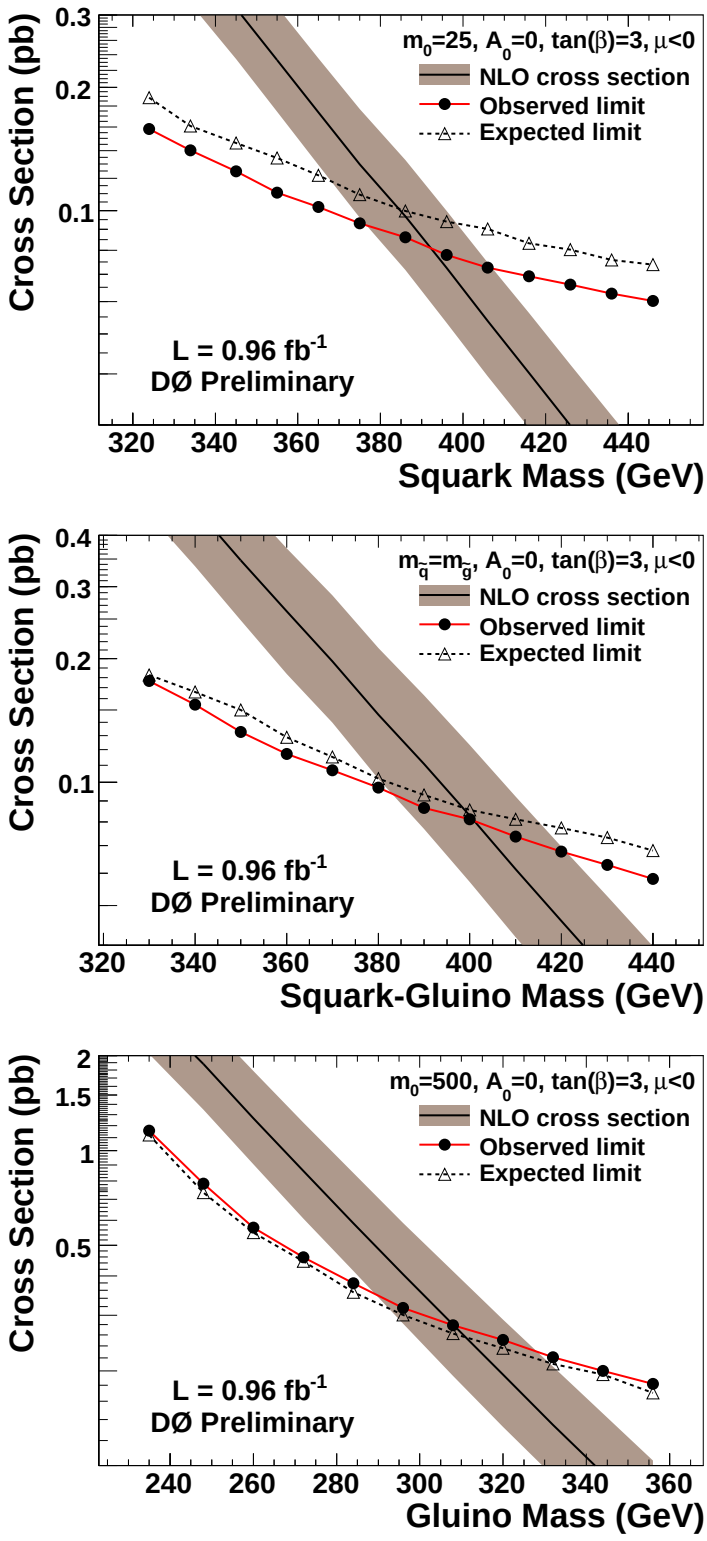

FIG. 4: For $\tan\beta = 3$, $A_0 = 0$, $\mu < 0$, observed (closed circles) and expected (opened triangles) 95% C.L. upper limits on the squark-gluino production cross section for $m_0 = 25\,\text{GeV}$ (top), $m_{\tilde{q}} = m_{\tilde{g}}$ (middle), and $m_0 = 500\,\text{GeV}$ (bottom). The nominal cross sections for squark and gluino pair production are also shown, with shaded bands corresponding to the PDF and renormalization-and-factorization scale uncertainties.

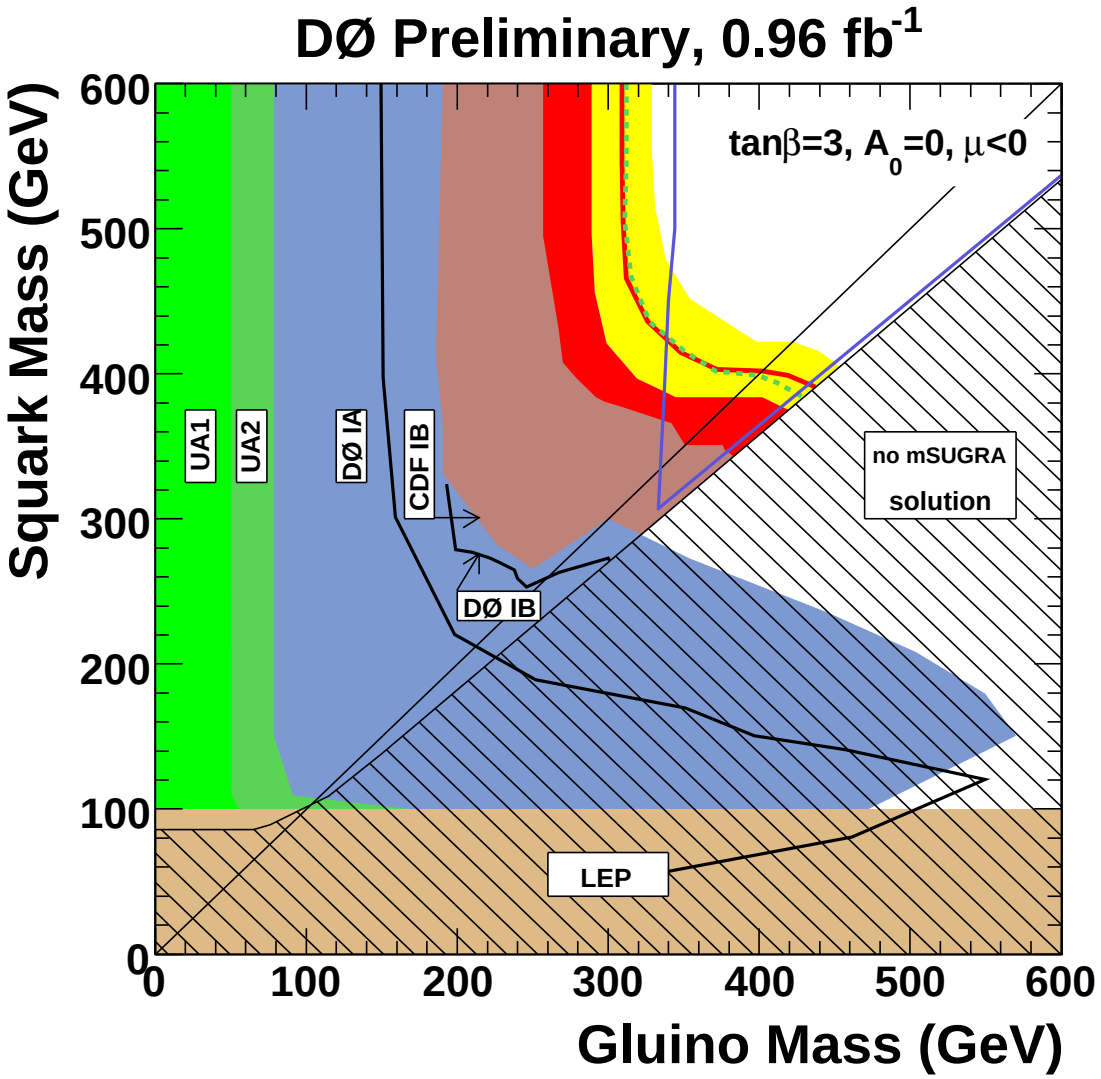

FIG. 5: In the squark and gluino mass plane, regions excluded by this analysis at the 95% C.L. in the mSUGRA framework for $\tan\beta = 3$, $A_0 = 0$, $\mu < 0$. The red line shows the excluded region for the central PDF and renormalization and factorization scale, $\mu_{\rm rf} = Q$. The corresponding expected limit is the dashed green line. The yellow band shows the effect of the PDF uncertainties and of varying $\mu_{\rm rf}$ by a factor of two. The DØ RunII results [2] with $310\,{\rm pb}^{-1}$ for the nominal cross section hypothesis correspond to the brown region. Regions excluded by previous experiments are indicated [21–25]. There is no mSUGRA solution in the black hashed region. The two thin blue lines indicate the indirect limits inferred from the LEP2 chargino and slepton searches [26].

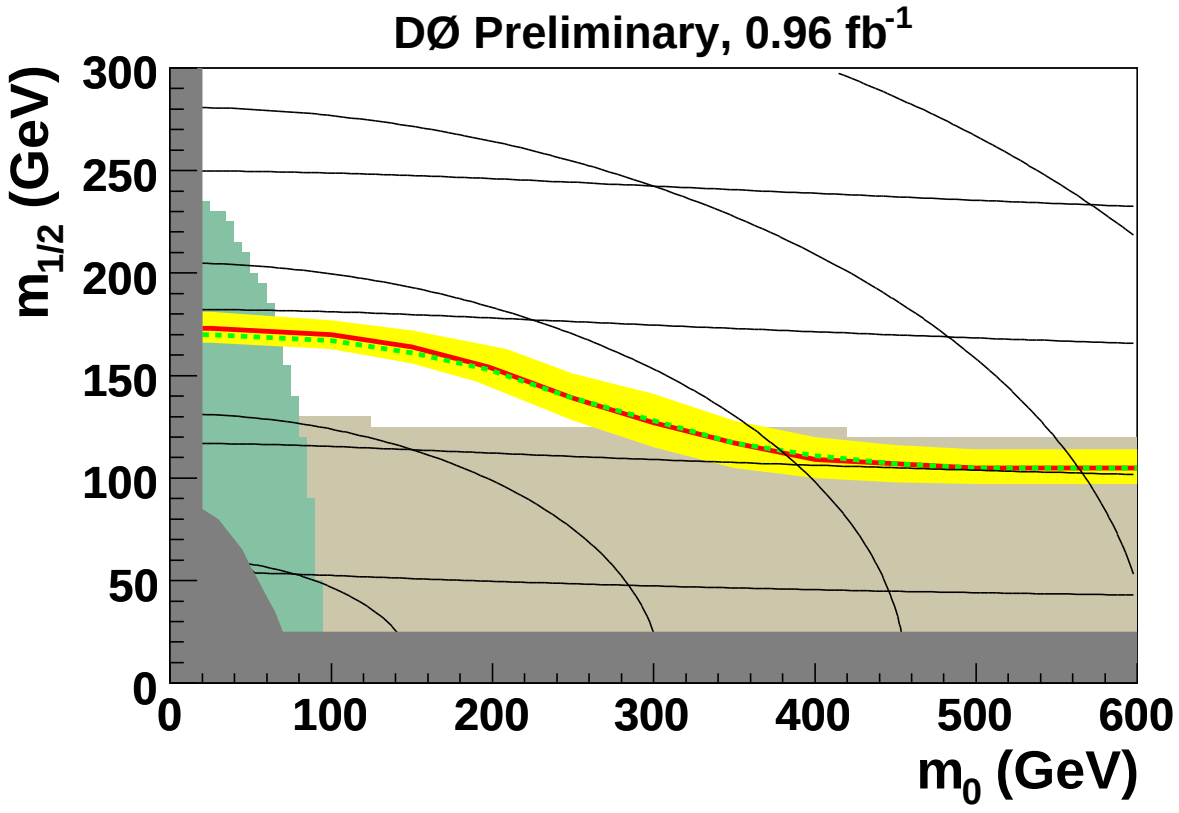

FIG. 6: In the $(m_0, m_{1/2})$ plane, regions excluded by this analysis at the 95% C.L. in the mSUGRA framework for $\tan\beta = 3$, $A_0 = 0$, $\mu < 0$. The red line shows the excluded region for the central PDF and renormalization and factorization scale, $\mu_{\rm rf} = Q$. The corresponding expected limit is the dashed green line. The yellow band shows the effect of the PDF uncertainties and of varying $\mu_{\rm rf}$ by a factor of two. There is no mSUGRA solution in the dark grey region. The beige and green regions are excluded by the LEP2 chargino and slepton searches [26], respectively. The nearly horizonthal thin black lines are the gluino iso-mass curves corresponding to gluino masses of 150, 300, 450, and 600 GeV. The other ones are squark iso-mass curves corresponding to squark masses of 150, 300, 450, 600, and 750 GeV.

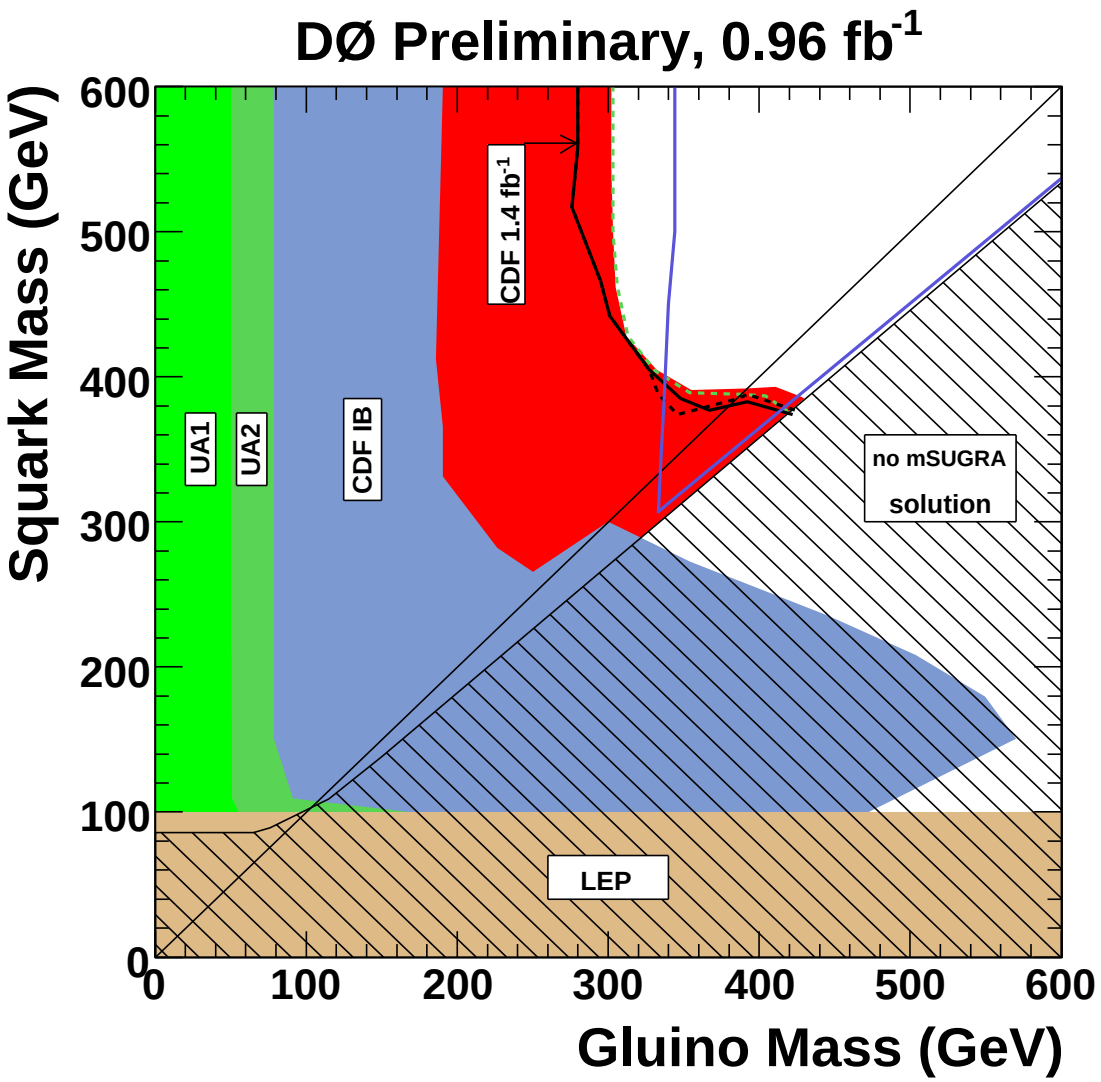

FIG. 7: Comparison of DØ and CDF [2] excluded regions at the 95% C.L. in the squark and gluino mass plane. Signal systematic uncertainties due to the PDF choice and to the renormalization and factorization scale are included in the limit computation in both cases. The red region is the excluded region observed by DØ. The corresponding expected limit is the dotted green line. The black and dotted black lines correspond to the CDF observed and expected limits, repectively. These limits are valid for the mSUGRA parameters $\tan\beta = 3$, $A_0 = 0$, $\mu < 0$ for DØ, and $\tan\beta = 5$, $A_0 = 0$, $\mu < 0$ for CDF.